Proposal and Examination of Method of Water Removal from Gas Diffusion Layer by Applying Slanted Microgrooves inside Gas Channel in Separator to Improve Polymer Electrolyte Fuel Cell Performance

Yoshio UTAKA[a], Akira OKABE[b] and Yasuyuki OMORI[c]

[a] Faculty of Engineering, Yokohama National University

79-5 Tokiwadai, Hodogaya-ku, Yokohama, Kanagawa 240-8501, Japan

[b] Suzuki Motor

Co.300 Takatsuka-cho, Minami-ku, Hamamatsu-shi, Shizuoka 432-8611 Japan

[c] Toyota Motor Co.

1 Toyota-Cho, Toyota City, Aichi Prefecture 471-8571, Japan

* Corresponding author: Yoshio UTAKA

Tel. / fax: +81 45 339 3909.

E-mail address: utaka@ynu.ac.jp

Postal address: Faculty of Engineering, Yokohama National University, 79-5 Tokiwadai, Hodogaya, Yokohama 240-8501, Japan

Abstract

The objective of this study was to improve the management of moisture from the gas diffusion layer (GDL) in the gas channel of a separator for PEFC. At the cathode-side, oxygen is transported as reactant gas from gas channel through GDL. When large quantity of moisture is generated during high power generation, moisture blocks transport of oxygen, and the cell voltage drops drastically. Narrow microgrooves with axes at tilt angle to the air flow were arranged inside channel walls. The water from GDL was discharged along microgrooves to facing top of GDL by forces of capillary and air flow shearing. Laser induced fluorescence method was used to measure water velocity in microgrooves. The effect of air velocity in the gas channel on water velocity in microgrooves was investigated. It was shown microgrooves manufactured inside gas channel worked properly. Water velocity in microgrooves increased with increasing air velocity, and moisture could be discharged from GDL by applying microgrooves. Furthermore, effective length of the microgrooves needed to remove water from the GDL surface increased with decreasing inclination angle of microgrooves in the range of 20°– 45°. An effective length of approximately 200 mm was attained, which was overall length of experimental apparatus.

Key Words: Polymer Electrolyte Fuel Cell, Separator, Gas Channel, Water Management, Slanted Microgrooves, LIF Method

1. **Introduction**

Polymer electrolyte fuel cells (PEFCs) are expected to be used as power sources for automobiles, cogeneration power sources for homes, etc. because of their low environmental load, high power density, and ability to operate at low temperatures. As seen in the general structure of a PEFC, at the cathode side, oxygen is transported from the gas channel in the separator through the gas diffusion layer (GDL) to the catalyst layer. Similarly, at the anode side, hydrogen is transported from the gas channel through the GDL to the catalyst layer. The electric power is produced by the chemical reaction of oxygen and hydrogen at the catalyst layer. The cell voltage is reduced by flooding phenomena, dryout phenomena, etc. Flooding occurs as a result of the liquid water produced by the chemical reaction, which accumulates in the microporous media of the GDL and the GDL surface on the gas channel side at the cathode. Finally, the diffusion of the reaction gas is suppressed. On the other hand, the proton conductivity in the polymer electrolyte membrane is decreased by low humidity during dryout. Therefore, moisture management in a membrane electrode assembly (MEA) is very important to improve the performance of PEFCs. Thus, for appropriate liquid water management, it is necessary to remove the extra liquid water in the GDL on the cathode side, to prevent an over-accumulation of liquid water in the GDL and GDL surface in the gas channel at the cathode side of a PEFC.

The authors [1] proposed a new GDL configuration, in which two porous media with different wettabilities are alternated (a hybrid configuration). Additionally, the authors [2], [3], [4] confirmed that this hybrid configuration is effective by measuring the apparent oxygen diffusivity in micro-porous GDLs using a galvanic cell oxygen absorber, along with the simultaneous measurement of the effective oxygen diffusivity and X-ray computed tomography visualization of the liquid water in carbon paper-type GDLs. GDLs with a higher oxygen diffusivity and the presence of liquid water, such as the hybrid configuration, can realize a better liquid water management performance by the addition of a gas channel structure, which aims at preventing the accumulation of liquid water on the GDL surface. Focusing on the use of a separator for moisture control, previous studies have tested gas channels such as a parallel type or serpentine type. Tanigawa et al. [5], [6] examined the effect of a gas channel on the condensate behavior using numerical simulations of serpentine-type separators with different rib widths. Konomi et al. [7], [8] developed a hybrid separator that combined the interdigitated type [9] and parallel type to improve the performance of a PEFC. As mentioned above, various studies have been performed to examine different gas channel configurations. However, problems have been found. For instance, liquid water accumulates within the GDL just below the rib and near the point of contact between the side wall of the channel and the GDL surface. Thus, it is necessary to avoid the

accumulation of water near the rib. Kumbur et al. [10] examined the behavior of a liquid droplet, such as the contact angle and departure diameter. Zhang et al. [11] reported that liquid water can easily accumulate at the channel corner. Palan et al. [12] investigated the removal of liquid water using acoustic and vibrational methods. Further, Mench et al. [13] examined the effect of wettability on the inner surface of a channel by the visualization of liquid water using neutron radiography, and showed that the water removal performance is enhanced by combining a hydrophilic inner surface and hydrophobic GDL. Synchrotron X-ray tomography was used by Krüger et al. [14] to visualize the water distribution in the GDL and flow field channels of a PEMFC subsequent to operation. Visualizations of the water droplets and wetting layer formations in the flow field channels were shown. However, few studies have investigated ways to enhance liquid water removal by the configuration of the channel wall, as intended in this study.

In this study, in order to reduce the accumulation of liquid water on GDL surface, the authors proposed a method where thin microgrooves with axes at a tilt angle to the air flow were arranged at both the side and upper walls inside the gas channel, which was composed of the GDL surface and separator walls. Figure 1 (a) and (b) shows a schematic view of the liquid water distribution in the case of relatively hydrophilic walls. As shown in Fig. 1 (a), a liquid–gas two phase flow is formed in a conventional gas channel, and it is probable that liquid water accumulates on the GDL surface when a large quantity of water is produced. The objective of this study was to enhance the removal performance from the MEA to gas channel through the GDL. As shown in Fig. 1 (b), microgrooves with axes at a tilt angle are arranged at both the side and top walls inside a square cross section of the gas channel. The water flowing through and from upstream moves to the opposite top wall from the GDL through the microgrooves without accumulating on the GDL surface, by means of the air flow shearing and capillary force produced by the surface tension within the microgrooves. The effects of the air velocity in the gas channel, flow rate of the liquid water through the GDL, and tilt angle of the microgrooves were examined in this study.

2. Experimental apparatus and procedure

2.1 Configuration of microgrooves and experimental system

Figure 2 shows the structures of the microgrooves on the imitated separator wall made of acrylic plate, whose surface was good in water wettability. Their axes have a tilt angle to the air flow, and they are arranged at both the side and upper walls inside the gas channel. Table 1 lists the specifications of the microgrooves, where the symbols correspond to those denoted in Fig. 2. Two kinds of gas channels with square cross sections were used, with a width and height of d_g = 1.0 mm and 2 mm, respectively. In addition, microgrooves with axes at a tilt angle to the air flow

were arranged at the walls inside the gas channel. Moreover, a larger groove, which allowed liquid water to move in the direction of the gas flow, was arranged in the center of the upper wall. The widths and depths of the two microgrooves at both the side and upper walls were $d_1 = h_1 = 0.4$ mm and $d_1 = h_1 = 0.2$ mm, corresponding to d_g = 2.0 mm and 1.0 mm, respectively. The widths and depths of the groove at the center of the upper wall were $d_2 = h_2 =$ 0.5 mm and $d_2 = 0.3$ mm, $h_2 = 0.2$ mm for $d_1 = 0.4$ mm and $d_1 = 0.2$ mm, respectively. The tilt angle between the microgrooves and gas flow direction is represented by θ, and pitch of the microgrooves is represented by p. Experiments were carried out under the condition that tilt angle θ was set at 30° for $d_1 = h_1 = 0.4$ mm and at 20°, 30°, and 45° for $d_1 = h_1 = 0.2$ mm.

In order to examine the water removal performance in the gas channel with microgrooves described above, an experimental apparatus that simulated water production by a chemical reaction was fabricated. Figure 3 shows a schematic of the experimental system. The bottom wall of the gas channel was composed of the GDL, which was made of a micro-porous media (carbon paper) without PTFE treatment, and liquid water was supplied to the gas channel through the GDL. The surface of the microgrooves was made more wettable by a coating of titanium dioxide. Air flowed through the gas channel. The microgrooves were arranged at one side and the upper walls of the gas channel, while an acrylic opaque flat plate was installed at the other side wall to allow visual inspection. Considering the fact that flooding tends to easily occur downstream of the gas channel because of an increased flow rate, the length interval along the gas channel over which the microgrooves were arranged was 80 mm down the stream (the total length of the channel was 198 mm) in this study. A mini-tank for the liquid water supply under the GDL was attached, with a total length of 200 mm. Water was supplied to the gas channel through the GDL at a constant flow rate using a syringe pump. From the starting position of the liquid water supply, the x and l coordinates were set in the flow direction from the inlet of the channel and starting position of the microgrooves, respectively.

Furthermore, in order to clarify the behavior of the liquid water within the microgrooves, its surface velocity was measured using the laser induced fluorescence (LIF) method, as shown in the next section.

2.2 LIF method and image analysis

The LIF method was suitable for this study because it allowed the flow velocity to be evaluated without disturbing the liquid water within the narrow grooves. A high light sensitivity, long-term retention of coloring, color strength, and water solubility are required of a photochromic dye. A representative organic photochromic molecule with these characteristics is spironaphthooxazine sulfonate [15]. The coloring mechanism of a spironaphthooxazine

sulfonate solution, which was used as a photochromic dye in this study, is shown in detail in Fig.4. The bonding between the spiro-carbon and atomic oxygen was broken by ultraviolet radiation, and a ring-opened product was produced, which provided color. This ring-opened product rapidly returned to a ring-closed product and the color disappeared by heating or visible light radiation. An ultraviolet laser (with a wavelength of 337.1 nm) was periodically used with pulse duration of 0.8 ns to radiate a water solution of photochromic dye at the center of the microgrooves. The colored spot produced by the laser-induced fluorescence was photographed using a high-speed camera through a long-focusing microscope. The surface velocity of the liquid water flowing in the tilt direction within the microgrooves was calculated from the moving distance of the colored spots with elapsed time.

Figure 5 shows the colored images for $\theta = 30°$ and $d_1 = h_1 = 0.4$ mm. The velocities of the water surface in the microgrooves, which were filled completely with water as seen in Fig. 5, was measured, because it was confirmed the surface of grooves was wettable. Figure 6 (a) and (b) shows schematic views of the colored water within a microgroove, where the colored spot is shown as a closed circle moving with the water flow. Figure 6 (a) and (b) shows images just after coloring ($t = t_0$ s) and 3/60 s after coloring ($t = t_0 + 3/60$ s), respectively. Coloring occurred at the spot radiated by the laser. A comparison of Fig. 6 (a) and (b) confirms that the colored spot moves with the water flow in a microgroove. The area of coloring is elongated with the flow by the velocity distribution in the depth direction. In this study, based on images of the movements of colored spots, the luminance distributions were obtained from pictures just after coloring and at some point in time after coloring along the center line in the direction of the tilted microgroove on the side wall (red lines in Fig. 6). The surface velocity was calculated from the moving distance of the luminance distributions.

Figure 7 shows the variation in the luminance distributions, which was obtained by the deduction of the luminance of the background just before laser radiation from the luminance values of Fig. 6 (a) and (b), in order to resolve the non-uniform background lighting. For $t = t_0$ s and $t = t_0 + 3/60$ s, respectively, least square lines were fitted using the minimum value of luminance to zero. In addition, the intersections of the lines for the least square and zero luminance values, as shown by points a and b in Fig. 7, were adopted as the forefronts of coloring. Considering the fact that the points denoted by the same symbol in Figs. 6 and 7 correspond with each other, the distance between lines a and b was determined to be the moving distance of the liquid water surface. The surface velocity of the liquid water was calculated using Eq. (1):

$$V_{\mathrm{w}} = k \times \Delta x / \Delta t . \qquad (1)$$

where V_w is the surface velocity of the liquid water (mm/s), k is the image resolution (mm/pixel), Δx is the distance between lines a and b (pixel), and Δt is the elapsed time.

3. Results and discussion

Using a gas channel with microgrooves, experiments were carried out at a constant water supply flow rate. The flow density was 0.93 nL/(mm^{2}s), which was calculated using a current density I = 2.0 A/cm^2 corresponding to the large current range of an actual PEFC. The base width of the water generating area was assumed to be a gas channel of 1 mm and equal to the width beneath the rib.

Figure 8 shows the variations in the surface water velocity along the gas channel. The surface water velocity was measured using an LIF method at the center line of the microgroove, with a gas flow velocity range of 4.0–6.0 m/s. The scattering of the measured velocities was likely due to the non-uniformity of the water supply from the micro-porous layer, as well as the precision of the LIF measurement. Although this scattering was not small because of the micro-scale phenomena, the target in this study is adequately reached. The reproducibility of surface water velocity in the measurement were performed at several flow conditions. The maximum data spread of them was within 7 %. Figure 8 (a) and (b) shows the measured velocities corresponding to the two gas channel widths of 1 and 2 mm, with microgrooves of 0.4- and 0.2-mm square cross-sections, respectively. The horizontal coordinate l represents the distance from the starting position of the microgrooves (l = 0) along the gas channel. The surface water velocities in the microgrooves were measured for both channel cases. Here, there are the sections without data points around l = 20 mm in Figs. 8 and 9, because a columnar structure, which was removed later, prevented the observation in the initial stage of experiment. It can be seen that the surface water velocity in the microgroove decreased with increasing distance and then became almost constant downstream because of the effect of the water flow from upstream. The effectiveness of the shearing force of the gas flow and capillary (surface tension) effect on the liquid water moving within the microgrooves was confirmed. Since in each case of Fig. 8 (a) and (b), it was found that the surface velocity of the water within the microgroove increased with an increase in gas velocity, the effect of the gas shearing force was considered to play an important role in removing water. In addition, near the starting position of the microgrooves, the surface velocity of the water was large and became constant downstream. For each microgroove dimension, the surface velocities of the water downstream of the gas channel were 1–2 mm/s for a gas velocity of 4.0 m/s and 1.5–3 mm/s for a gas velocity of 6.0 m/s.

For a comparison of the effects of the dimensions of the gas channel and microgroove at the same gas velocity, re-plots of the measured values from Fig. 8 are shown in Fig. 9 (a) and (b). In the comparison between the 0.2- and 0.4-mm microgrooves, it was found that the effect of the microgroove dimension on the surface water velocity is not very explicit. It is desirable to adopt a 1-mm gas channel with a microgroove size of 0.2 mm from the standpoint of PEFC downsizing. Therefore, examinations of the water removal performance hereafter focus on the case with a microgroove width of 0.2 mm.

Figure 10 shows the variations in the surface velocity of the water against the total length of the gas channel (l = 0–80 mm) in the gas flow direction in the case of a microgroove with a width of 0.2 mm. The air flow velocity within the gas channel was V_g = 6.0 m/s, and the flow rate of the water supply was 0.93 nL/(mm^{2}s), which corresponded to a current density I = 2.0 A/cm^2 (the base value in this study). The tilt angles of the microgrooves θ were 20°, 30°, and 45°. As described above, the surface water velocity rapidly decreased around l = 0–10 mm and approached a constant value toward l = 30 mm, independently of the tilt angle of the microgrooves θ. The surface velocity of the water increased with decreasing tilt angle in the 20°–45°range in this study. In the case of θ = 45°, the surface velocity decreased with an increase in l, and the water was not able to rise up within the microgrooves of the side walls with a value of l larger than 12 mm. In the case of θ = 30°, liquid water began to overflow from the microgrooves at approximately l = 35 mm. It was confirmed for θ = 30° that the effective length was longer in comparison with θ = 45°. This phenomenon is called “flooding” hereafter. Here, the lengths without data plotted denote the sections of instable water behavior and/or minus velocity with instability, which was difficult to measure.

In the flooding region, the side walls were covered by a water film, and it was not easy to measure the surface velocity of the liquid water in the microgrooves. Since the water within the grooves at the upper wall was supplied both from upstream and through the microgrooves of the side walls, its flow rate increased with an increase in the gas flow direction. Therefore, the liquid water within the microgrooves of the side walls had difficulty flowing into the grooves at the upper wall with increasing l. The flow at the upper wall was likely to be unstable with an increasing water flow rate. The liquid removal limit produced by unstable flow was considered to be strongly dependent on the driving force for the water flow on the upper wall by the shearing of the air flow. In the case of θ = 20°, the surface velocity of the water along the microgrooves was measured throughout gas channel l = 0–80 mm, and no liquid removal bound was observed. That is, since the surface velocity of the water showed larger positive values, it was possible to consider that the supplied water could be transferred through the microgrooves and removed from the

GDL surface. The effective length was secured throughout the gas channel. Thus, a microgroove of θ = 20° had a favorable performance for water removal.

Figure 11 shows the effect of the water supply rate under θ = 20° and V_g = 6.0 m/s. $Q_{I=2.0}$ and $Q_{I=4.0}$ correspond to I = 2.0 A/cm^2 and I = 4.0 A/cm^2 in the PEFC power generation, respectively. The open symbols show the cases having a proper rising flow of water within the microgrooves. The closed squares show the cases with a downward flow of water within the microgrooves because of flooding. In the case of $Q_{I=2.0}$, no water accumulation on the GDL surface was observed throughout l = 0–80 mm. However, in case of $Q_{I=4.0}$, flooding occurred mechanically downstream of the gas channel because the flow rate of the liquid water supply was doubled. After a thin film was generated at about l = 35 mm (associated with flooding), water began to flow back within the microgrooves, and liquid water accumulated on the GDL surface at the bottom of the gas channel from about l = 60 mm.

When the channel height (1mm in this study) is lowered, which is advantageous in realizing a compact PEFC, the gradient of gas velocity near the wall increases and also a larger gas velocity becomes necessary to keep equal flow rate of reactant gas. Accordingly, since it is possible to holdback the water strongly up against the wall facing the GDL with the effect of microgrooves due to higher shearing force and velocity of gas, it will be possible to apply the microgrooves to a smaller channel height. Thus, it is possible to predict that microgrooves with a 0.2 mm square cross-section and a tilt angle of 20° can be used for stack dimensions of an actual PEFC even under a condition of greater water generation that corresponds to a high current density of 2.0 A/cm^2, because it was possible to remove the water with microgrooves in an approximately 200-mm-long gas channel throughout the experiment.

4. Conclusions

In order to control water in the gas channel on the cathode side of a PEFC, a separator was proposed that contained a gas channel with tilted microgrooves, which had cross-sections of 0.4 mm and 0.2 mm square. It was confirmed that water could be removed from the GDL surface toward the opposite upper wall due to the capillary force (surface tension) and shearing of the gas flow. The surface velocities of the water within the microgrooves were measured using the LIF method under various conditions. The following results were obtained.

(1) It was confirmed that liquid water was removed from the GDL surface along the microgrooves, and the proposed method of liquid water removal was effective, based on surface water velocity measurements using the LIF method.

(2) The surface velocity of the water increased with an increase in the gas velocity and decrease in the tilt angle of the microgrooves. It was 2– 8 mm/s under gas velocities of 4 and 6 m/s with 0.2-mm square microgrooves.

(3) In the case of 0.2-mm square microgrooves, the surface velocity of the liquid water increased, and the water removal performance was enhanced by a decrease in the tilt angle in the gas flow direction for 20°, 30°, and 45°.

(4) It is possible to predict that microgrooves with a 0.2 mm square cross-section and a tilt angle of 20° can be used for stack dimensions of an actual PEFC even under a condition of greater water generation that corresponds to a high current density of 2.0 A/cm^2, because it was possible to remove the water with such microgrooves in-approximately 200 mm long gas channel throughout the experiment.

Acknowledgments

This work was supported in part by a Grant-in-Aid for Scientific Research [(B) 20360096] from the Japan Society for the Promotion of Science (JSPS) and the Strategic International Collaborative Research Program of the Japan Science and Technology Agency (JST). The authors would like to thank Professor Yasushi Yokoyama at Yokohama National University for his valuable instruction on the synthesis of photochromic dye.

References

[1] Utaka, Y., Hirose, I. and Tasaki, Y., Characteristics of Oxygen Diffusivity and Water Distribution by X-ray Radiography in Microporous Media in Alternate Porous Layers of Different Wettability for Moisture Control in Gas Diffusion Layer of PEFC, *International Journal of Hydrogen Energy*, Vol.36 (2011), pp. 9128-9138.

[2] Utaka, Y., Tasaki, Y., Wang, S., Ishiji, T. and Uchikoshi, S., Method of Measuring Oxygen Diffusivity in Microporous Media, *International Journal of Heat and Mass Transfer*, Vol.52 (2009), pp. 3685-3692.

[3] Koresawa, R. and Utaka, Y., Precise Measurement of Effective Oxygen Diffusivity for Microporous Media Containing Moisture by Review of Galvanic Cell Oxygen Absorber Configuration, *International Journal of Heat and Mass Transfer*, (2014), (accepted).

[4] Koresawa, R. and Utaka, Y., Improvement of Oxygen Diffusion Characteristics in Gas Diffusion Layer with Planer-distributed Wettability for Polymer Electrolyte Fuel Cell, *Journal of Power Sources*, Vol.**, Issue * (2014), pp.***-***(in press).

[5] Tanigawa, H., Miyazaki, Y. and Tsuruta, H., Effect of Gas Channel on Water Formation in Polymer Electrolyte Fuel Cell: 1st Report, Two-Dimensional Analyses with Lattice Gas Automaton Method, *Transactions of the Japan Society of Mechanical Engineers, Ser.B,* Vol.75, No.759 (2009), pp. 186-191.

[6] Tanigawa, H., Miyazaki, Y. and Tsuruta, H., Effect of Gas Channel on Water Formation in Polymer Electrolyte Fuel Cell: 2nd Report, Experimental and Three-Dimensional Analyses with Lattice Gas Automaton Method, *Transactions of the Japan Society of Mechanical Engineers, Ser.B,* Vol.75, No.759 (2009), pp. 192-198.

[7] Konomi, T., Kitahara, T., Nakajima, H., Tashiro, M. and Takazono, Y., Development of a PEFC with Parallel Hybrid Pattern Gas Channels: 1st Report, Design and Performance Test of the Gas Channels, *Transactions of the Japan Society of Mechanical Engineers, Ser.B,* Vol.74, No.741 (2008), pp. 3-10.

[8] Konomi, T., Kitahara, T., Nakajima, H., Tashiro, M. and Takazono, Y., Development of a PEFC with Parallel Hybrid Pattern Gas Channels: 2nd Report, Performance and Flooding under the Rib of Interdigitated Gas Channels, *Transactions of the Japan Society of Mechanical Engineers*, Ser.B, Vol.74, No.741 (2008), pp. 11-17.

[9] Wood, III, D.L., Yi, J.S. and Nguyen, T.V., Effect of Direct Liquid Water Injection and Interdigitated Flow Field on the Performance of Proton Exchange Membrane Fuel Cells, *Electrochimica Acta*, Vol.43, No.24 (1998), pp. 3795-3809.

[10] Kumbur, E.C., Sharp, K.V. and Mench, M.M., Liquid Droplet Behavior and Instability in a Polymer Electrolyte Fuel Cell Flow Channel, *Journal of Power Sources*, Vol.161 (2006), pp. 333-245.

[11] Zhang, F.Y., Yang, X.G. and Wang, C.Y., Liquid Water Removal from a Polymer Electrolyte Fuel Cell, *Journal of the Electrochemical Society*, Vol.153, (2006), pp. A225-A232.

[12] Palan, V., Shepard Jr., W.S. and Williams, K.A., Removal of Excess Water in a PEM Fuel Cell Stack by Vibrational and Acoustical Methods, *Journal of Power Sources*, Vol.161 (2006), pp. 1116-1125.

[13] Turuhan, A., Kim, S., Htzell, M. and Mench, M., Impact of Channel Wall Hydrophobicity on Through-plane Water Distribution and Flooding Behavior in a Polymer Electrolyte Fuel Cell, Electrochimica Acta, Vol.55 (2010), pp.2734-2745.

[14] Krüger, Ph., Markötter, H., Haußmanna, J., Klages, M., Arlt, T., Banhart, J., Hartniga, Ch., Manke, I. and Scholta, J., Synchrotron X-ray Tomography for Investigations of Water Distribution in Polymer Electrolyte Membrane Fuel Cells, *Journal of Power Sources*, Vol.196 (2011), pp. 5250-5255.

[15] Maeda, S., Spirooxazines, in Organic Photochromic and Thermochromic Compounds, Vol. 1, Ed by Crano, J.C. and Guglielmetti, R.J., pp. 85-109, Plenum Press, New York (1999).

Figure Captions

Fig. 1 Schematic of water behavior through microgrooves from GDL

(a) Conventional separator without microgrooves

(b) Separator with microgrooves

Fig. 2 Details of structure of separator with microgrooves

(a) Over view

(b) Cross-sections and dimensions

Fig. 3 Schematic of experimental system

Fig. 4 Chemical structure of photochromic dye

Fig. 5 Aspect of photochromic reaction in a microgroove

(a) $t = t_0$ s

(b) $t = t_0$+3/60 s

Fig. 6 Schematic of photochromic reaction with water movement

(a) $t = t_0$ s

(b) $t = t_0$+3/60 s

Fig. 7 Variation of luminance distribution

Fig. 8 Variation of surface water velocity against flow distance: effect of gas velocity ($Q_{I=2.0}$ = 0.93 nL/(mm^{2}s) and θ = 30°)

(a) Microgroove of d_1 = 0.4 mm

(b) Microgroove of d_1 = 0.2 mm

Fig. 9 Variation of surface water velocity against flow distance: effect of microgroove dimension ($Q_{I=2.0}$ = 0.93 nL/(mm^{2}s) and θ = 30°)

(a) Air velocity of 4.0 m/s

(b) Air velocity of 6.0 m/s

Fig. 10 Variation of water velocity in micro-grooves against distance (d_1 = 0.2 mm, θ = 20°, 30°, 45°)

Fig. 11 Variation of water velocity in micro-grooves against distance (d_1 = 0.2 mm, I = 2.0 and 4.0 A/cm^2)

Table Caption

Table 1 Specification of separator with microgrooves

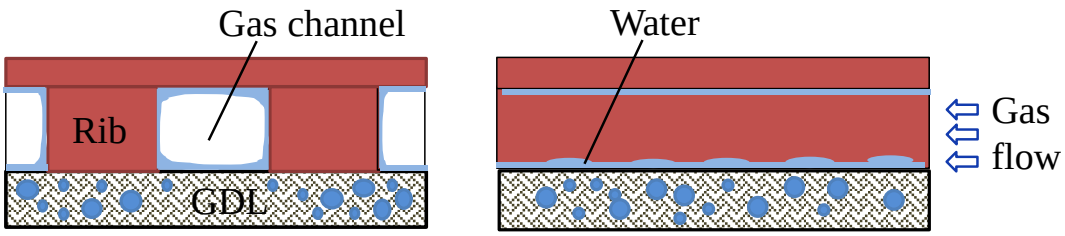

(a) Conventional separator without microgrooves

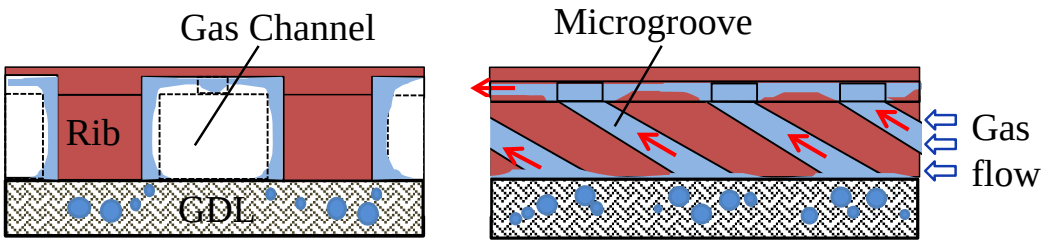

(b) Separator with microgrooves

Fig .1 Schematic of water behavior through microgrooves from GDL

Table 1 Specification of separator with microgrooves

d_g mm	θ°	P mm	d_1 mm	h_1 mm	d_2 mm	h_2 mm
2.0	30	1.6	0.4	0.4	0.5	0.5
1.0	45	0.57	0.2	0.2	0.3	0.2
	30	0.8				
	20	1.17				

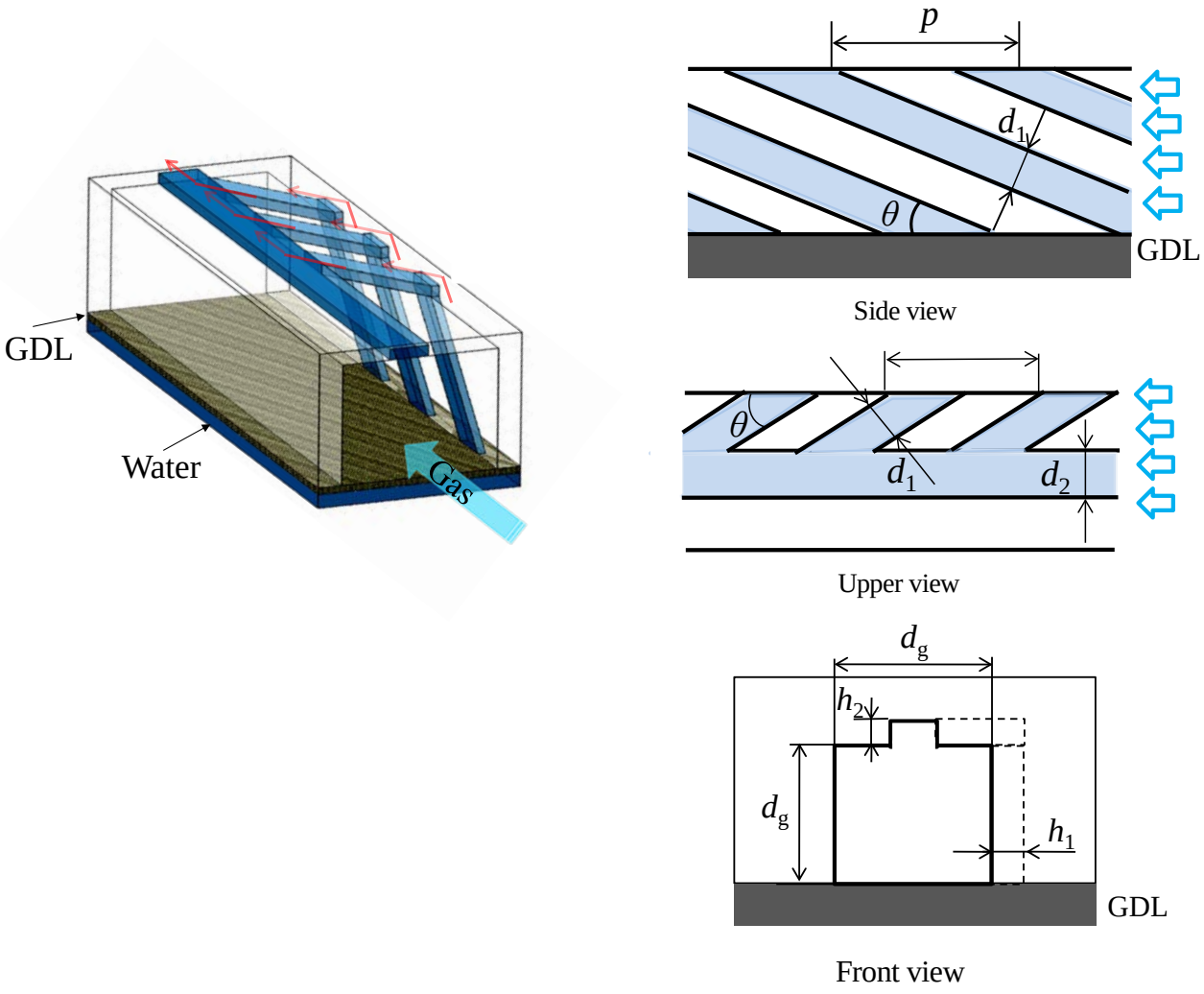

(a) Overview (b) Cross-sections

Fig.2 Details of structure of separator with microgrooves

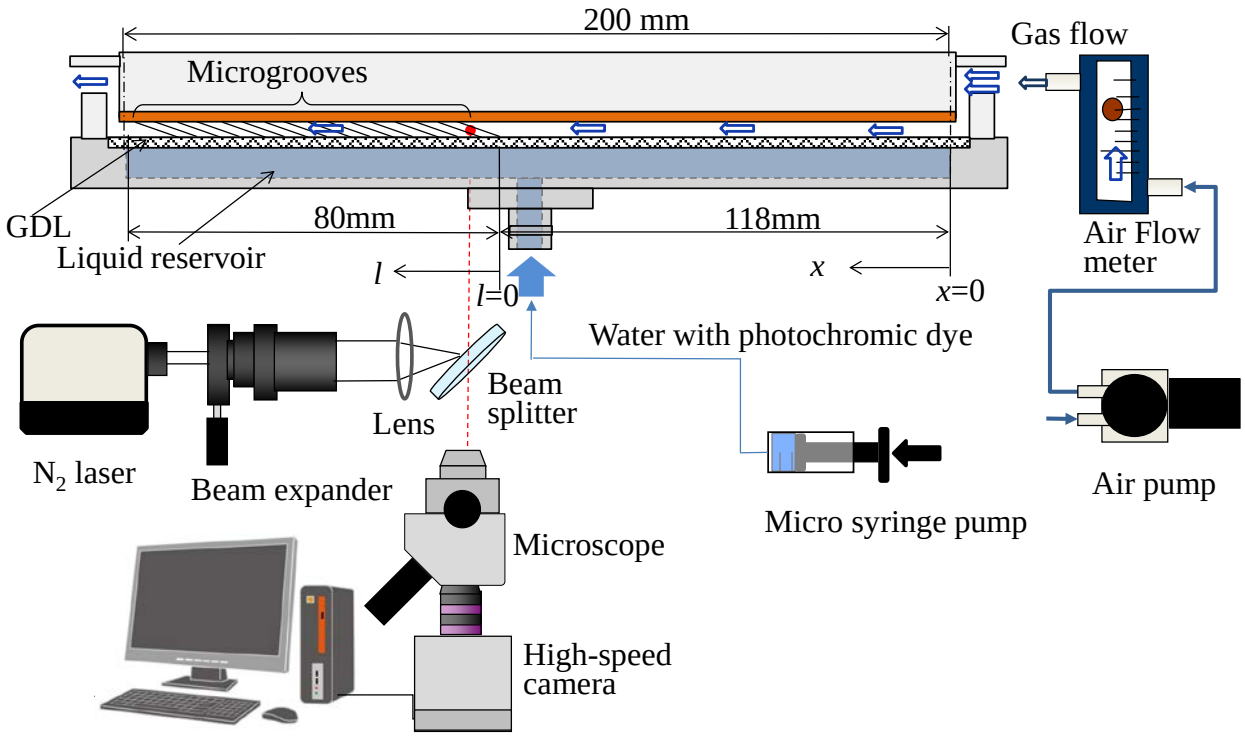

Fig.3 Schematic of experimental system

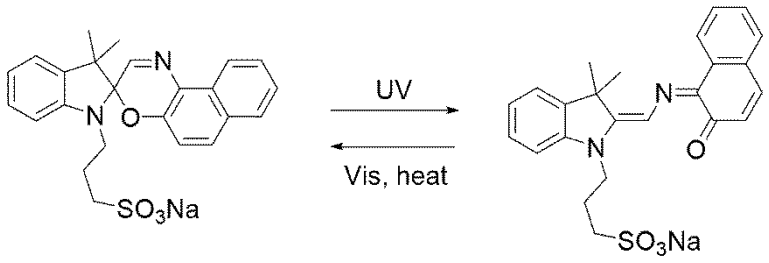

Colorless Blue

Spironaphthooxazine sulfonate
(sodium 3-[1-(3,3-dimethylspiro[indoline-2,3’
-[3H]naptho[2,1-b][1,4]oxazine])]propanesulfonate)

Fig.4 Chemical structure of photochromic dye

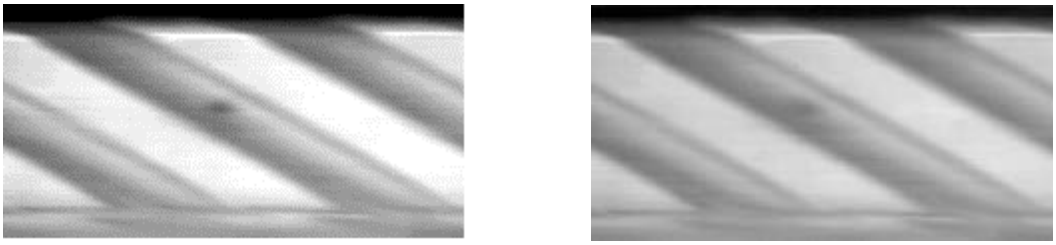

(a) $t = t_0$ s (b) $t = t_0$+3/60 s

Fig.5 Aspect of photochromic reaction in a microgroove

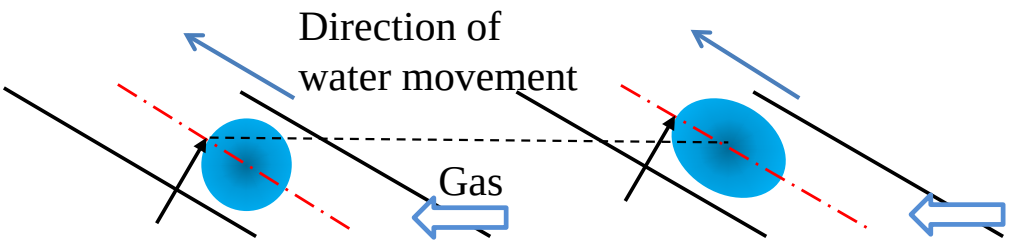

(a) $t = t_0$ s (b) $t = t_0$+3/60 s

Fig.6 Schematic of photochromic reaction with water movement

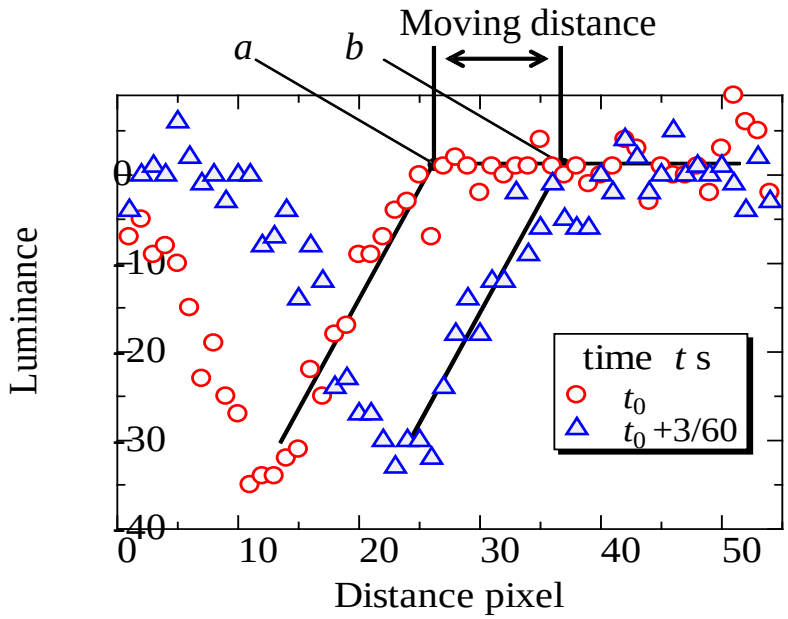

Fig.7 Variation of luminance distribution

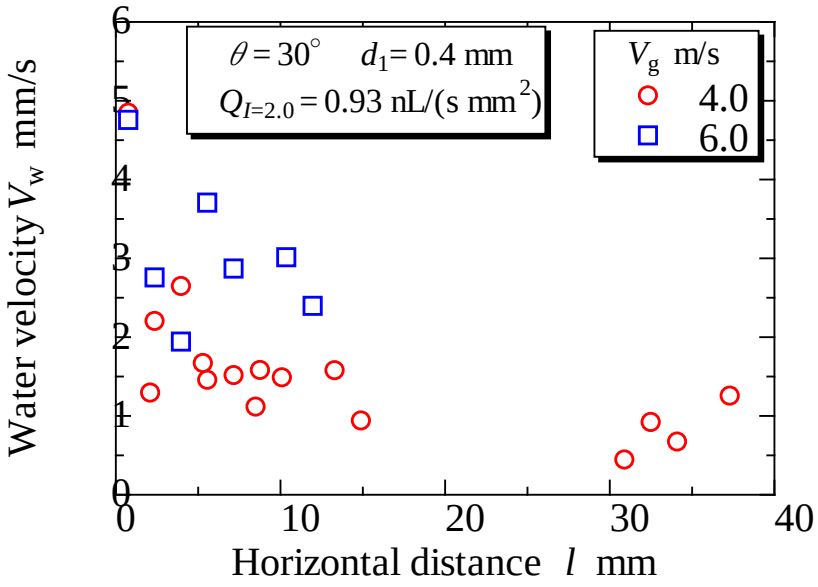

(a) Microgroove of d_1 = 0.4 mm

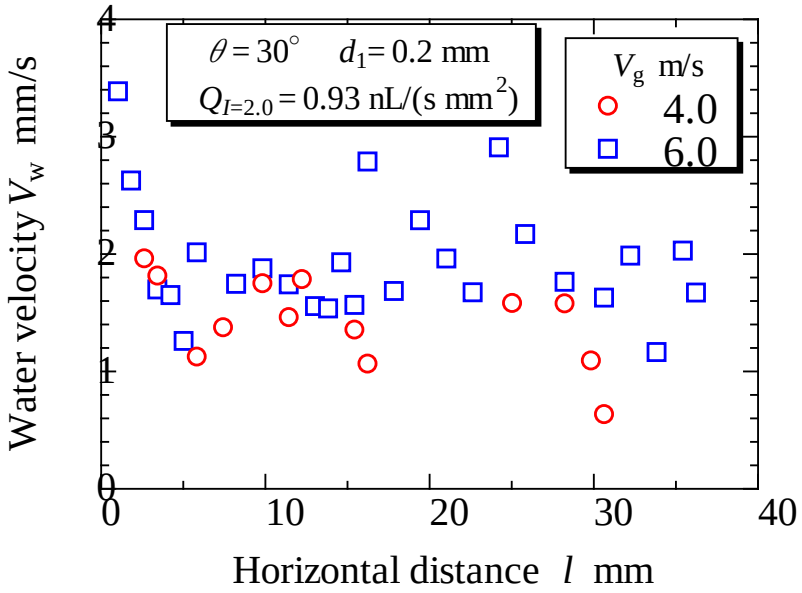

(b) Microgroove of d_1 = 0.2 mm

Fig.8 Variation of surface water velocity against flow distance: effect of gas velocity ($Q_{I=2.0}$ = 0.93 nL/(mm^{2}s) and θ = 30°)

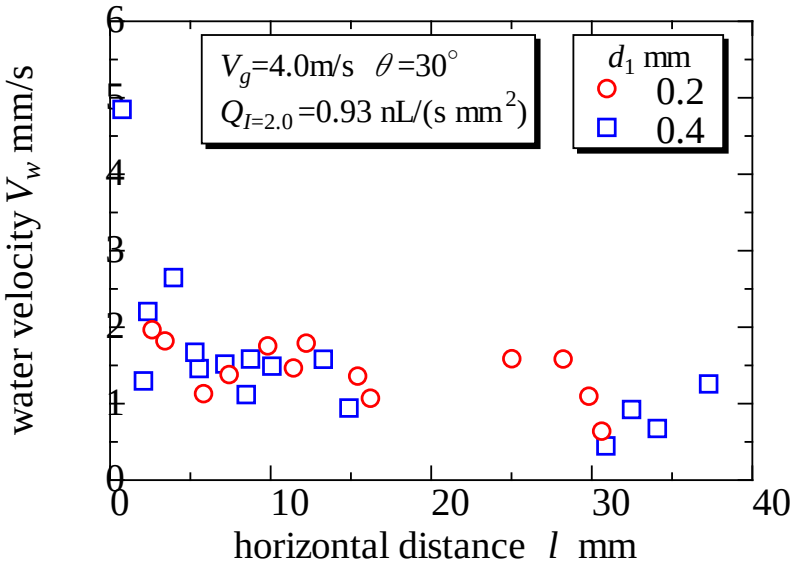

(a) Air velocity of 4.0 m/s

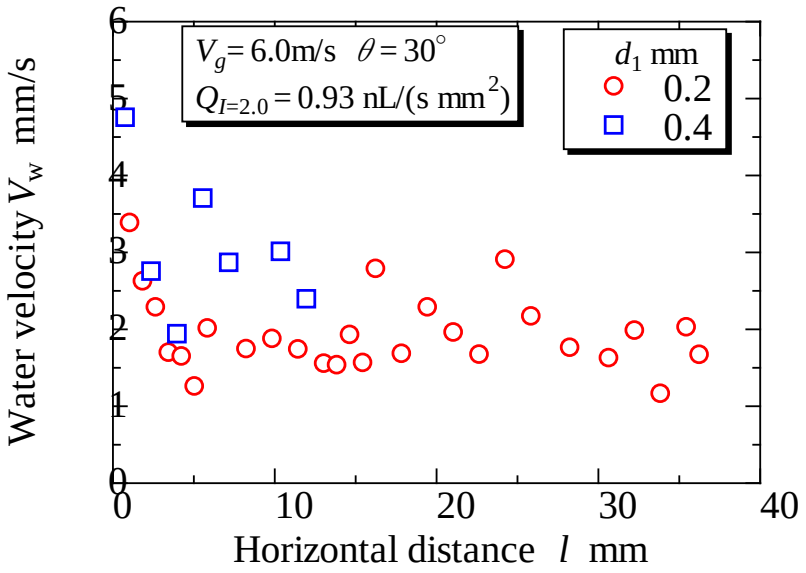

(b) Air velocity of 6.0 m/s

Fig.9 Variation of surface water velocity against flow distance: effect of microgroove dimension ($Q_{I=2.0}$ = 0.93 nL/(mm^{2}s) and θ = 30°)

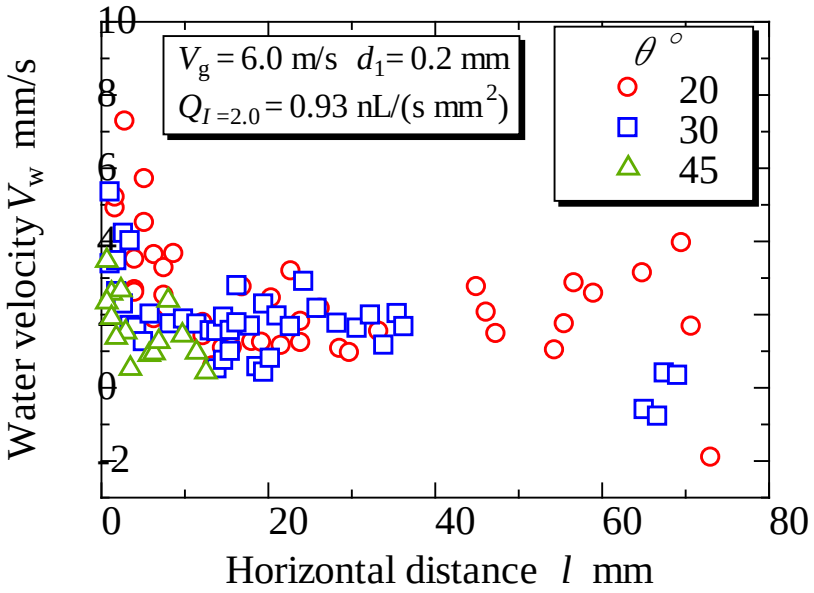

Fig.10 Variation of water velocity in microgrooves against distance (d_1 = 0.2 mm, θ = 20°, 30°, 45°)

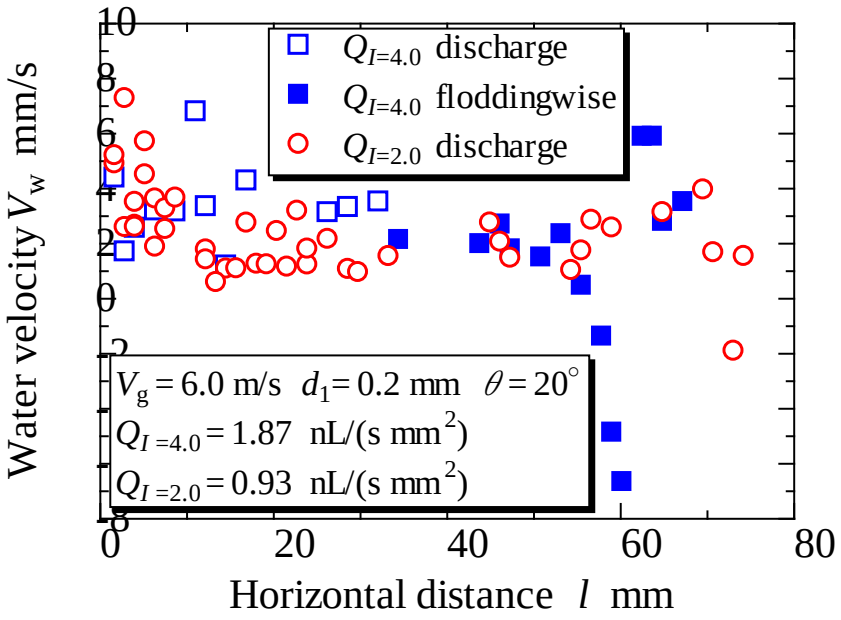

Fig. 11 Variation of water velocity in microgrooves against distance (d_1 = 0.2 mm, I = 2.0 and 4.0 A/cm^2)